Extreme Mechanics Letters 15 (2017) 26–37

Contents lists available at ScienceDirect

Extreme Mechanics Letters

journal homepage: www.elsevier.com/locate/eml

On the efficiency of piezoelectric energy harvesters

Zhengbao Yang [a,*], Alper Erturk [b], Jean Zu [a]

[a] Department of Mechanical and Industrial Engineering, University of Toronto, Toronto, ON, M5S 3G8, Canada
[b] G.W. Woodruff School of Mechanical Engineering, Georgia Institute of Technology, Atlanta, GA 30332, USA

ARTICLE INFO

Article history:
Received 14 March 2017
Received in revised form
5 May 2017
Accepted 9 May 2017
Available online 10 May 2017

Keywords:
Energy harvesting
Piezoelectric
Efficiency
Energy conversion
Vibration

ABSTRACT

Energy harvesting is an essential technology for enabling low-power, maintenance-free electronic devices, and thus has attracted a great deal of attention in recent years. A variety of designs and approaches have been proposed to harvest ambient vibration energy, but crucial questions remain regarding figures of merit characterizing the performance of energy harvesters. Of primary importance is the energy conversion efficiency. There are large discrepancies in the definition and tested values of efficiency in the literature. This study is intended to answer the fundamental question for energy harvesters: how to define and calculate the energy conversion efficiency. We first review studies on efficiency and analyze the energy flow in an energy harvesting system. Based on the analysis, we derive an efficiency expression for linear cantilever energy harvesters. The developed efficiency expression transparently and quantitatively reveals the relationship between efficiency and key parameters. Experiments are performed to validate the efficiency expression. Furthermore nonlinear energy harvesters are tested in both on-resonance and off-resonance conditions. Both experimental and theoretical studies manifest that the energy conversion efficiency tends to decrease as the excitation frequency rises and its value is related to the phase difference between excitations and responses. Around resonance states where the phase difference of both linear and nonlinear energy harvesters is about 90 degrees, the efficiency calculation is much simplified.

1. Introduction

The dramatic decrease in power consumption of electronic components sets a stage for autonomous operation by using the energy harvesting technology [1–3]. Harvesting mechanical energy from ambient vibration and deformation via the piezoelectric effect has been intensively studied in the past decades. Researchers have recently focused on improving the performance of piezoelectric energy harvesters (PEHs) via high-performance piezoelectric materials [4–8], structure & manufacturing process innovation [9–14] and optimization of dynamic characteristics [15–17].

In order to optimize PEHs' performance, appropriate performance metrics need to be defined first. Taking various structural, material and vibration parameters into account, researchers have proposed several comprehensive figures of merit including normalized power density (NPD) [18], effectiveness [19,20], volume figure of merit (FoMv) [21] and systematic figure of merit with bandwidth information ($SFoM_{BW}$) [22]. Although these metrics, developed under some assumptions, provide comprehensive information on PEHs' performance, basic metrics such as power output and efficiency are still preferred by both researchers and end users. The ultimate goal of research on PEHs is to generate as much electrical energy as possible from a mechanical vibration source, that is, high power output and high efficiency. While the electrical power output can be measured in experiments and calculated in theoretical models, the mechanical power input cannot be easily monitored and there is no unified calculation process. As a consequence, a large discrepancy exists in the reported efficiency values. As Table 1 lists, it has been estimated that efficiency can be over 80% [23,24]; it has also been argued that efficiency cannot exceed 50% no matter how well an energy harvester is optimized [25]. Some researchers claimed that efficiency around the resonance state is much higher than that in off-resonance states [26], while others believed that efficiency decreases monotonically as the excitation frequency increases [27].

Efficiency is not only a critical metric for the development and optimization of PEHs, but also has been widely used to compare PEHs with other power generation methods (e.g., solar panels, thermal energy harvesters, triboelectric nano-generators, etc.). Therefore, it is essential to understand efficiency, the fundamental performance metric of energy harvesters. In this paper, we present an insight into the PEHs' efficiency in the full frequency range both theoretically and experimentally.

* Corresponding author.
E-mail address: hityzb@gmail.com (Z. Yang).

http://dx.doi.org/10.1016/j.eml.2017.05.002
2352-4316/

Table 1
Reported efficiency values of various piezoelectric energy harvesters.

Reference	Efficiency	Note
[23]	∼50%–90%	PZT; bimorph cantilever; vibration; theoretical estimation
[24]	>80%	PZT; tube; flow-induced vibration; theoretical estimation
[28]	2.56%	PVDF film; rainbow bimorph; theoretical estimation
[29]	21.8%	PVDF nanofiber; direct deformation; experimental data
[30]	7.5%	PZT; flextensional structure; direct deformation; experimental data
[31]	>80%	PZT; fixed–fixed bimorph plate; theoretical estimation
[32]	∼7%	PZT; cantilever; vibration; experimental data
[33]	0.72%	PZT; cantilever; fluid flows experimental data
[4]	5.4%/14.9%/27.5%	PZT/PMN-PT/PZN-PT; cantilever; vibration; experimental
[34]	<44%	PZT; bimorph cantilever; vibration; theoretical estimation
[35]	3.1%	PZT sandwiched between two Terfenol-D discs
[36]	1.2%	PZT; Impact-type using a rotational flywheel; experimental data
[26]	26%/<2%	PZT cantilever beam; vibration; on-resonance/off-resonance; experimental data
[37]	12.47%	PVDF/AlO-rGO beam; direct deformation; experimental data
[38]	80.3%/35.1%/15.4%	Stack/Membrane/Cantilever; ball drop impact; experimental data
[39]	10%	PZT fixed–fixed beam; ball drop impact; experimental data
[40]	5%–18%	Piezoelectric nanowires: direct deformation; experimental data

Efficiency, also called energy conversion efficiency, generally refers to the ratio of the output energy to the input energy of a system. To maintain consistency, it makes sense to define efficiency of PEHs in the same way, i.e., the ratio between the output electrical energy E_{out} and the input mechanical energy E_{in} ($\eta = E_{out}/E_{in}$). This definition is in a form similar to the electromechanical coupling factor squared k_{ij}^2, where k_{ij} is the material coupling factor (electrical field in direction i, stress in direction j). However, the value of k_{ij} from piezoelectric material suppliers represents how efficient the employed piezoelectric element (piezoelectric material alone) is in terms of converting mechanical energy into electrical energy and it does not account for the structural design and electrical circuit aspects. Therefore, the material coupling factor k_{ij} cannot be applied to the entire structure. The overall harvester efficiency η is usually much smaller than the material coupling factor k_{ij}. The concept of coupling factor, or the coupling coefficient, has also been defined at the system level [41] for the piezoelectric structure as $k_{sys}^2 = (\omega_o^2 - \omega_s^2)/\omega_o^2$, where ω_o and ω_s are, respectively, the open-circuit and short-circuit natural frequencies of the vibration mode of interest (note that $k_{sys}^2 = \kappa^2/(1+\kappa^2)$, where κ^2 is defined as an electromechanical coupling coefficient in the following sections. It is widely used in the energy harvesting literature [27,42,43]). The system coupling coefficient k_{sys} is a measure of mechanical to electrical energy conversion within the lossless structure and is not equal to the efficiency η either since it does not account for the presence of an electrical load as well as mechanical and dielectric losses.

While most researchers have reached an agreement on the definition of efficiency ($\eta = E_{out}/E_{in}$), the expressions of the input and output energy vary, which leads to a large discrepancy in the reported efficiency values. In this paper, we analyze the dynamic characteristics of the input and output power of both linear and nonlinear PEHs in detail. It is found that the phase difference between the excitation and the response significantly affects the input energy, and further the efficiency of the system.

In the following, we first review some representative work on efficiency. We then analyze the energy flow of the energy harvesting process and derive an algebraic efficiency expression based on a universal SDOF model. Following that, an experiment is conducted to validate the developed efficiency expression. Via the developed model, we discuss the effect of different parameters on the energy conversion efficiency. Finally, the phase responses of nonlinear PEHs are studied experimentally.

2. Literature review

Piezoelectric energy conversion efficiency has been discussed for a long time. In 1990s, Goldfarb and Jones [44] studied the efficiency of a piezoelectric stack energy harvester under a steady-state sinusoidal compressive force. They proposed a linear circuit model without accounting the hysteresis phenomenon to analyze the effect of different parameters on efficiency. The experiments indicated that large-amplitude and low-frequency force with a high load resistance tends to achieve high efficiency. A maximum efficiency around 10% was obtained at approximately 5 Hz (several orders of magnitude below the resonance frequency of the piezoelectric stack). It is noteworthy that piezoelectric stacks are not practical to be used directly as energy harvesters without any auxiliary structures due to their ultra-high stiffness. By contrast, beam + inertial mass configurations, thanks to their flexible characteristics, receive the most attention. Most recently proposed models are based on the beam configurations.

In 2004, Richards et al. [42] derived an exact efficiency formula based on a simplified SDOF model.

$$\eta = \frac{1}{2}\frac{\kappa^2}{1-\kappa^2}\Bigg/\left(\frac{1}{Q} + \frac{1}{2}\frac{\kappa^2}{1-\kappa^2}\right). \tag{1}$$

In Eq. (1), efficiency η depends only upon the quality factor Q and the electromechanical coupling coefficient κ^2 of the whole system. This definition only works at the resonance state with a matching resistance. The theoretical study estimated that the efficiency value can be over 90% with the assumed weak damping and strong coupling effects, which high value has seldom been achieved in experiments. Nevertheless, the exact formula reveals the effects of damping and electromechanical coupling on efficiency.

In 2006, Shu and Lien [27] theoretically analyzed the energy conversion efficiency of a cantilever PEH coupled with a full-bridge rectifier around resonance states. They assumed that the input mechanical energy was the sum of extracted electrical energy and the energy dissipated by the structure damping. The efficiency expression was

$$\eta = \frac{\alpha\kappa^2}{\zeta\left(\alpha\tilde{\omega} + \pi/2\right)^2 + \alpha\kappa^2}. \tag{2}$$

Efficiency is dependent upon the frequency ratio $\tilde{\omega}$ (response frequency/natural frequency), the normalized resistance α (load resistance/matching resistance), the electromechanical coupling coefficient κ^2 and the mechanical damping ratio ζ. In general, the conversion efficiency can be improved with a large coupling coefficient and a small damping ratio. It is known that, due to the stiffness difference of piezoelectric elements between the short-circuit condition (natural frequency $= 1$) and the open-circuit condition (natural frequency $= \sqrt{1+\kappa^2}$), the frequency to obtain the maximum power output shifts along the variation

of the coupling factor. Therefore, the analysis was classified into two categories: weak coupling and strong coupling. Maximum efficiency of 46% and >80% were estimated to be reached by the defined weak and strong coupling systems, respectively.

It is worth mentioning that the assumed strong coupling system has seldom been made in experiments. Most experimental efficiency values are much lower than the estimated value [32]. The same expression has also been derived in different ways [25,45].

In 2009, Liao and Sodano [46] argued that the classic definition of efficiency did not provide information on the capacity of a PEH for converting mechanical energy to electrical energy. All systems with low damping ratios showed high efficiency, irrespective of the mechanical-to-electrical energy conversion performance. Therefore they proposed to redefine the efficiency of PEHs as the ratio of power output to strain energy over each cycle. The energy conversion efficiency was redefined as

$$\eta_{PH} = \frac{\kappa^2 \alpha \tilde{\omega}}{1 + (1+\kappa^2)(\alpha\tilde{\omega})^2}. \tag{3}$$

In this definition, the efficiency value is not related to the structural damping. The numerical study estimated a maximum efficiency of ∼2.5%, attained around the system resonance frequency. Off-resonance efficiency is way smaller than the on-resonance efficiency. There is no experimental validation in the study. The authors did not give an explicit way to measure the defined strain energy in experiments. Hence this definition has not been widely used. Furthermore, it is inconvenient to compare PEHs with other energy harvesting methods by the re-defined metric η_{PH}. The metric η_{PH}, similar to the loss factor used for structural damping, reflects the mechanical-to-electrical energy conversion of PEHs in a certain aspect, but cannot replace the role of efficiency.

In 2014, Shafer and Garcia [25] presented a theoretical analysis on the efficiency of a base-excited bimorph cantilever coupled with a full-bridge rectifier. They found that energy was transferred back and forth between the energy harvester and excitation source over each cycle. For some systems (e.g., backpacks, shoes), energy transferred back to the excitations was thought to be impossible to be recovered. The authors thus defined two cases: conservative and non-conservative. For the conservative case, the defined efficiency was the same as that in Eq. (2); for the non-conservative case, a complex expression was derived

$$\eta_{nc} = \frac{\kappa^2 \alpha \tilde{\omega}}{(\alpha\tilde{\omega} + \pi/2)^2} \frac{1}{\sqrt{\psi}} \frac{1}{\xi(\theta)}, \tag{4}$$

where ψ and $\xi(\theta)$ account for information of the modal response and phase difference, respectively.

The efficiency vs. frequency response curve exhibited three peaks and, and at the resonance states efficiency had an upper limit 44%. The three-peak response has seldom been found in experiments and is different from that in Ref. [27] where efficiency is defined in the same way. The difference is deemed to be from that, in the theoretical study herein, the efficiency value at each frequency was calculated with a load resistance actively changing to maximize power output.

In 2015, Kim et al. [23] presented another efficiency expression for a base-excited cantilever PEH with a resistive load.

$$\eta = \frac{\alpha\kappa^2}{2\xi\left(1 + \alpha^2\tilde{\omega}^2\right) + \alpha\kappa^2}. \tag{5}$$

They argued that efficiency has no limit and can be over 80% under certain circumstances. There is no experimental validation in the paper. The developed model indicated that the optimal resistance to get the maximum power output was different from that to obtain the highest efficiency, which was also discussed in Refs. [25,46].

3. Theoretical analysis

In terms of the working principle, PEHs can be classified into two types: inertial energy harvesters and non-inertial energy harvesters. For non-inertial energy harvesters, force directly applies to the systems and causes active materials to expand or shrink. For inertial energy harvesters, excitations do not deform the active materials directly, but induce inertial force in the systems. Such energy harvesters are usually fixed on a vibration base such as human bodies, animals, vehicles and buildings. In this paper we mainly focus on inertial energy harvesters.

3.1. Energy flow analysis

Before modeling an energy harvesting system, we first need to comprehend the energy flow in the system. Physically, an energy harvesting system involves three parts: an excitation source such as human motion or vehicle vibration, an energy harvesting device and an interface circuit. Overall, there are four energy reservoirs and three steps of energy transformations in the process as shown in Fig. 1.

Step 1. Mechanical energy is captured and transferred from the excitation source to the PEH.
Step 2. Mechanical energy is converted to the electrical energy in the PEH.
Step 3. Electrical energy is extracted from the PEH to the external load.

Each energy reservoir couples with its neighbors in both forward and reverse directions. The first reservoir refers to the mechanical energy in the host. The effect of adding a PEH should be trivial to the dynamic characteristics of the host. (e.g., vehicles and building sensors). That means the excitation energy overall is infinite relative to the energy used by the following energy harvesting system. The second reservoir contains oscillating kinetic energy of the inertial mass, elastic potential energy of the structure and structural damping energy. The third reservoir stores electrical energy in a PEH, which cannot be fully extracted by the external electrical load. The fourth reservoir represents the electrical energy used by the electrical load. In the whole process, a part of energy is inevitably transferred to heat due to a variety of effects such as structural damping, dielectric loss and current leakage, etc.

As a dynamic system, a PEH experiences an oscillating energy flow. Therefore, we should consider the stable state and the net energy transformation in each step while analyzing the energy transmission process. Following the classic efficiency definition, efficiency ought to be equal to the ratio of the net input energy to the 4th reservoir and that to the 2nd reservoir.

3.2. Electromechanically coupled model

We choose the most widely used cantilever PEH as the study object. The PEH consists of a unimorph beam with one end fixed at the excitation source, and the other end attached with a mass block (Fig. 2). This electromechanical coupling system is modeled as an equivalent lumped-parameter SDOF dynamic system (Fig. 3) with the dynamic equations

$$m\ddot{X} + c\dot{X} + kX + \theta V = -m\ddot{Z}, \tag{6}$$

$$C_p\dot{V} + \frac{1}{R}V = \theta\dot{X}, \tag{7}$$

where m, c, k, C_p, R and θ are the equivalent mass, damping, stiffness, piezoelectric internal capacitance, external resistance and piezoelectric coupling factor, respectively. V is the output

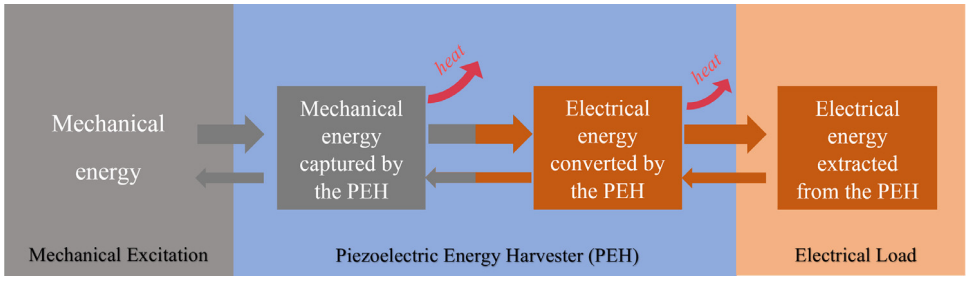

Fig. 1. Energy flow in an piezoelectric energy harvesting system.

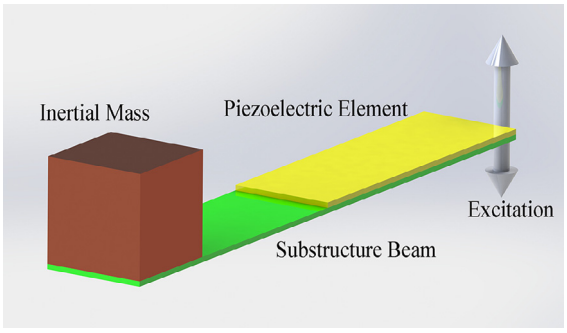

Fig. 2. A cantilever piezoelectric energy harvester under a base excitation.

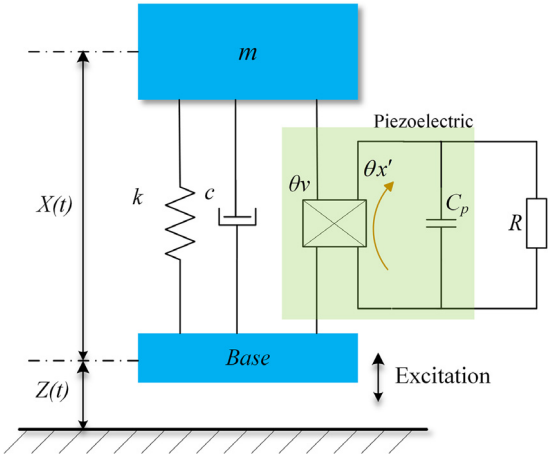

Fig. 3. Schematic of a piezoelectric energy harvesting system.

voltage over the piezo element. X is the relative displacement and Z is the base excitation. $\dot{()}$ represents differentiation to time "t". The value of the coupling factor θ can be identified by either theoretical analysis [34,47,48] or experimental method [49]. The governing equations can be derived from the piezoelectric constitutive equations and Euler–Bernoulli beam theory, and have been used for analyzing different PEHs [34,47,50–53]. Note that the developed model does not account for the dielectric loss in piezoelectric materials, and it does not work under ultra-low frequency conditions.

A variety of electrical circuits have been proposed to treat the AC current from PEHs, including various DC–DC converter topologies [54,55], SSHI [56], SSHI-MR [57], SECE [58], OSECE [59], bias-flip interface circuit [60], single-supply pre-biasing circuit [61] and so on. Each of them shows its own characteristics and has different effects on the energy flow. Without loss of generality, we here consider the simplest scenario: connecting PEHs with a resistor. This is also the most commonly discussed circuit in the literature. Efficiency of different energy harvesting circuits can be found in the book [62]. We would not talk about it here.

To simplify the solving process, we introduce the following non-dimensional variables into the governing equations,

$$\tau = \omega_n t, \qquad \tilde{\omega} = \frac{\omega}{\omega_n}, \qquad \xi = \frac{c}{2m\omega_n},$$
$$\kappa^2 = \frac{\theta^2}{kC_p}, \qquad \alpha = \frac{1}{RC_p\omega_n},$$

where ω_n is natural angular frequency ($\omega_n = \sqrt{k/m}$); $\tilde{\omega}$ is frequency ratio; ξ is the damping ratio, κ^2 is the coupling coefficient. It is increasingly recognized that most practical applications of PEHs are with small coupling coefficients. Here we also introduce $r = 1/RC_p\omega = \alpha/\tilde{\omega}$, named resistance ratio, into the system. The maximum power is extracted by the external electrical load at the impedance matching condition, that is, $r = 1$ (weak coupling systems). The solutions below can be greatly simplified with the resistance ratio 'r'.

The nondimensional governing equations are

$$\begin{aligned} &x'' + 2\xi x' + x + \kappa^2 v = -z'' \\ &v' + \alpha v = x', \end{aligned} \tag{8}$$

where $x = X$, $z = Z$, $v = C_pV/\theta$, and $()'$ is differentiation to the nondimensional time "τ".

The harmonic base excitation is expressed as

$$z'' = A\cos(\tilde{\omega}\tau), \tag{9}$$

which can also be expressed as $\ddot{Z} = \omega_n^2 A\cos(\omega t)$.

Assume responses are also harmonic at the same frequency as that of the excitation.

$$\begin{aligned} &x = x_1\sin(\tilde{\omega}\tau) + x_2\cos(\tilde{\omega}\tau) \\ &x' = x_1\tilde{\omega}\cos(\tilde{\omega}\tau) - x_2\tilde{\omega}\sin(\tilde{\omega}\tau) \\ &x'' = -x_1\tilde{\omega}^2\sin(\tilde{\omega}\tau) - x_2\tilde{\omega}^2\cos(\tilde{\omega}\tau), \end{aligned} \tag{10}$$

$$\begin{aligned} &v = v_1\sin(\tilde{\omega}\tau) + v_2\cos(\tilde{\omega}\tau) \\ &v' = v_1\tilde{\omega}\cos(\tilde{\omega}\tau) - v_2\tilde{\omega}\sin(\tilde{\omega}\tau). \end{aligned} \tag{11}$$

Submitting Eqs. (9)–(11) into Eq. (8), we get

$$\begin{aligned} &-x_1\tilde{\omega}^2\sin(\tilde{\omega}\tau) - x_2\tilde{\omega}^2\cos(\tilde{\omega}\tau) \\ &\quad +2\xi\left[x_1\tilde{\omega}\cos(\tilde{\omega}\tau) - x_2\tilde{\omega}\sin(\tilde{\omega}\tau)\right] + x_1\sin(\tilde{\omega}\tau) \\ &\quad +x_2\cos(\tilde{\omega}\tau) + \kappa^2\left[v_1\sin(\tilde{\omega}\tau) + v_2\cos(\tilde{\omega}\tau)\right] \\ &\quad = -A\cos(\tilde{\omega}\tau) \\ &v_1\tilde{\omega}\cos(\tilde{\omega}\tau) - v_2\tilde{\omega}\sin(\tilde{\omega}\tau) + \alpha\left[v_1\sin(\tilde{\omega}\tau) + v_2\cos(\tilde{\omega}\tau)\right] \\ &\quad = \left[x_1\tilde{\omega}\cos(\tilde{\omega}\tau) - x_2\tilde{\omega}\sin(\tilde{\omega}\tau)\right]. \end{aligned} \tag{12}$$

Then, equating the coefficients of $\sin(\tilde{\omega}t)$ and $\cos(\tilde{\omega}t)$ on both sides, we have

$$\begin{aligned} &x_1\tilde{\omega}^2 + x_2 2\xi\tilde{\omega} - x_1 - \kappa^2 v_1 = 0 \\ &x_2\tilde{\omega}^2 - x_1 2\xi\tilde{\omega} - x_2 - \kappa^2 v_2 = A \\ &v_2\tilde{\omega} - \alpha v_1 = x_2\tilde{\omega} \\ &v_1\tilde{\omega} + \alpha v_2 = x_1\tilde{\omega}. \end{aligned} \tag{13}$$

The solutions are

$$x_1 = -\frac{2\xi\tilde{\omega} + \frac{\alpha\kappa^2\tilde{\omega}}{\tilde{\omega}^2+\alpha^2}}{\Lambda}A; \qquad x_2 = \frac{\tilde{\omega}^2 - 1 - \frac{\kappa^2\tilde{\omega}^2}{\tilde{\omega}^2+\alpha^2}}{\Lambda}A, \tag{14}$$

$$v_1 = \frac{\alpha\tilde{\omega} - (\alpha+2\xi)\tilde{\omega}^3}{\Lambda(\tilde{\omega}^2+\alpha^2)}A; \qquad v_2 = \frac{\tilde{\omega}^4 - (1+2\xi\alpha+\kappa^2)\tilde{\omega}^2}{\Lambda(\tilde{\omega}^2+\alpha^2)}A, \tag{15}$$

where $\Lambda = \left(\tilde{\omega}^2 - 1 - \frac{\kappa^2\tilde{\omega}^2}{\tilde{\omega}^2+\alpha^2}\right)^2 + \left(2\xi\tilde{\omega} + \frac{\alpha\kappa^2\tilde{\omega}}{\tilde{\omega}^2+\alpha^2}\right)^2 = \left(\tilde{\omega}^2 - 1 - \frac{\kappa^2}{1+r^2}\right)^2 + \left(2\xi\tilde{\omega} + \frac{\kappa^2 r}{1+r^2}\right)^2$.

3.3. Mechanical response

The displacement response is

$$x = X_{ap}\cos(\tilde{\omega}\tau + \phi_x), \tag{16}$$

where the displacement amplitude and the phase difference are

$$X_{ap} = \sqrt{x_1^2 + x_2^2} = \frac{1}{\sqrt{\Lambda}}A, \tag{17}$$

$$\phi_x = \tan^{-1}\frac{x_1}{x_2} = \tan^{-1}\frac{\tilde{\omega}\left(2\xi + \frac{\alpha\kappa^2}{\tilde{\omega}^2+\alpha^2}\right)}{\frac{\kappa^2\tilde{\omega}^2}{\tilde{\omega}^2+\alpha^2} + 1 - \tilde{\omega}^2} = \tan^{-1}\frac{\tilde{\omega}\left(2\xi + \frac{\kappa^2 r}{1+r^2}\right)}{\frac{\kappa^2}{1+r^2} + 1 - \tilde{\omega}^2}. \tag{18}$$

The magnification factor is

$$M = \frac{X_{ap}}{D_{base}} = \frac{\tilde{\omega}^2}{\sqrt{\left(\tilde{\omega}^2 - 1 - \frac{\kappa^2}{1+r^2}\right)^2 + \left(2\xi\tilde{\omega} + \frac{\kappa^2 r}{1+r^2}\right)^2}}, \tag{19}$$

where $D_{base} = A/\tilde{\omega}^2$ is the displacement amplitude of the base excitation.

For the short-circuit condition, we let the load resistor $R \to 0$, then we have

$$M_{R\to 0} = \frac{\tilde{\omega}^2}{\sqrt{\left(\tilde{\omega}^2 - 1\right)^2 + (2\xi\tilde{\omega})^2}}. \tag{20}$$

$M_{R\to 0}$ reaches the maximum value when $\tilde{\omega} = \sqrt{1-2\xi^2} \approx 1$, which is usually defined as the resonance frequency. For the open-circuit condition, we let the load resistor $R \to \infty$, then we have

$$M_{R\to\infty} = \frac{\tilde{\omega}^2}{\sqrt{\left(\tilde{\omega}^2 - 1 - \kappa^2\right)^2 + (2\xi\tilde{\omega})^2}}. \tag{21}$$

$M_{R\to\infty}$ reaches the maximum value when $\tilde{\omega} = \sqrt{1+\kappa^2-2\xi^2} \approx \sqrt{1+\kappa^2}$, which is known as the anti-resonance frequency. Resonance and anti-resonance points are very close to each other in low-frequency and weak-coupling circumstances.

Fig. 4 shows the phase angle at different excitation frequency points. Before the resonance state, the response tends to keep a same pace with the excitation. After the resonance state, the response tends to keep an opposite pace with the excitation. Around the resonance point, a phase shift of 90° occurs no matter what the damping ratio is. ϕ_x is in the range [0° 180°]. If the coupling coefficient $\kappa = 0$, the phase difference is the same as the expression for the mechanical SDOF systems (Eq. 3.77 in Ref. [63]).

3.4. Electrical response

We express the voltage response as

$$v = v_1\sin(\tilde{\omega}\tau) + v_2\cos(\tilde{\omega}\tau) = V_{ap}\cos(\tilde{\omega}\tau + \phi_v). \tag{22}$$

From Eq. (15), we get the response amplitude and phase difference

$$V_{ap} = \frac{\tilde{\omega}}{\sqrt{\tilde{\omega}^2+\alpha^2}}X_{ap} = \frac{\tilde{\omega}}{\sqrt{\tilde{\omega}^2+\alpha^2}}\frac{1}{\sqrt{\Lambda}}A$$
$$\phi_v = \tan^{-1}\frac{v_1}{v_2} = \tan^{-1}\frac{\alpha\tilde{\omega} - (\alpha+2\xi)\tilde{\omega}^3}{\tilde{\omega}^4 - (1+2\xi\alpha+\kappa^2)\tilde{\omega}^2}. \tag{23}$$

The power consumed by the external resistor is calculated as

$$P_{out} = \frac{\left(\theta v/C_p\right)^2}{R} = \frac{\theta^2}{C_p^2 R}\frac{\tilde{\omega}^2}{\tilde{\omega}^2+\alpha^2}X_{ap}^2\cos^2(\tilde{\omega}\tau + \phi_v) = \frac{\theta^2}{C_p^2 R}\frac{1}{1+r^2}X_{ap}^2\cos^2(\tilde{\omega}\tau + \phi_v). \tag{24}$$

The frequency of the power response is upgraded to 2ω and thus the cycle period becomes $T = 2\pi/2\omega$. The electrical energy generated per cycle is

$$E_{out} = \int_0^{\frac{2\pi}{2\omega}} P_{out}dt = \frac{\pi}{\omega}\frac{V_{RMS}^2}{R} = \frac{\pi}{2}\frac{\theta^2}{C_p}\frac{r}{1+r^2}X_{ap}^2, \tag{25}$$

where V_{RMS} refers to the root mean square voltage.

3.5. Input mechanical energy

Unlike the calculation process of the output electrical energy, the input mechanical energy does not have a uniform definition. A typical wrong definition is $P_{in} = F \times \left(\dot{X} + \dot{Z}\right) = m \times \ddot{Z} \times \left(\dot{X} + \dot{Z}\right)$. This definition goes against the facts in two ways. First, the excitation force from the host to the PEH cannot be expressed as mass multiplying acceleration. Supposing that the excitation acceleration is kept constant in a full frequency range, the acting force between the PEH and the host structure should keep constant based on this definition. However, the fact is that the acting force increases significantly around the resonance state. Secondly, velocity in the power definition should refer to the velocity of the point the force applied to, and it must be in the direction of the force. The velocity of tip mass in a PEH is not the one of the excitation point. Energy input to the PEH is from the point fixed on the excitation. The velocity of the point is, therefore, the velocity of the excitation source $\dot{Z}$.

There are three ways to define the input mechanical power.

Case 1: $P_{in} = F \times \dot{Z} = m \times \ddot{Z} \times \dot{Z}$.

Some assume that the whole structure vibrates at a same acceleration as the host's. This assumption is not appropriate because there are relative motions in the system.

Case 2: $P_{in} = F \times \dot{Z} = m \times \ddot{X} \times \dot{Z}$.

As the model in Fig. 2 indicates, a spring, a damper and a piezo element are connected with the excitation base. Thus the force of the load point is assumed to be equal to the damping force + the spring force + the piezo force, which is also equally applied to the tip mass, that is, $m \times \ddot{X}$. Therefore, the input power can be expressed as

$$P_{in} = -\frac{1}{2}m\omega_n^2 A X_{ap}\omega\sin(2\omega t + \phi_x) + \frac{1}{2}m\omega_n^2 A X_{ap}\omega\sin(\phi_x) = \frac{1}{2}m\left(\ddot{X}\right)_{amp}\left(\dot{Z}\right)_{amp}\left(-\sin(2\omega t + \phi_x) + \sin(\phi_x)\right). \tag{26}$$

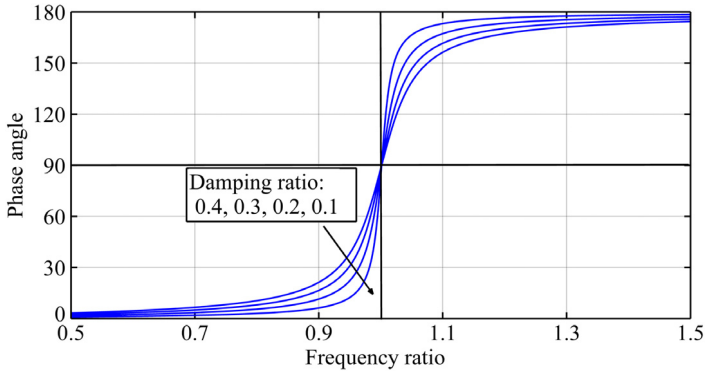

Fig. 4. Variations of phase angle ϕ_x with the frequency ratio $\tilde{\omega}$. The coupling coefficient $\kappa^2 = 0.0078$.

If there is no relative displacement ($X = 0$), the tip mass moves along with the base. The acceleration of the tip mass is equal to that of the base. That means the tip mass experiences a periodic force. However, no relative displacement means no spring, damping or piezo force, that is, no force applied to the mass block. The self-contradiction indicates that this equation does not reflect the real situation.

Case 3: $P_{in} = F \times \dot{Z} = m \times \left(\ddot{X} + \ddot{Z}\right) \times \dot{Z}$.

In this case, we do not face the self-contradiction issue in Case 2. If there is no relative motion, the tip mass moves along with the base at an acceleration of $\ddot{Z}$. The applied force is equal to the mass times the absolute acceleration.

$$\begin{aligned} P_{in} &= -\frac{1}{2}m\omega_n^2 A X_{ap}\omega \sin(2\omega t + \phi_x) \\ &\quad + \left[\frac{1}{2}m\omega_n^2 A X_{ap}\omega \sin(\phi_x)\right] + m\frac{\omega_n^4 A^2}{2\omega}\sin(2\omega t) \\ &= \frac{1}{2}m\left(\ddot{X}\right)_{amp}\left(\dot{Z}\right)_{amp}\left(-\sin(2\omega t + \phi_x) + \sin(\phi_x)\right) \\ &\quad + m\frac{\omega_n^4 A^2}{2\omega}\sin(2\omega t). \end{aligned} \tag{27}$$

There are sinusoidal functions in the power response equations, of which average value is zero per period. The effective value is only from the constant term $\sin(\phi_x)$. Comparing Case 2 and Case 3, we can find that the net input power is same, although the Case 3 shows a higher oscillation amplitude.

Using Eq. (27), we examine the power flow in both on- and off-resonance conditions. Three conditions are considered here, case 1: $\tilde{\omega} = 0.5$, case 2: $\tilde{\omega} = 1$, case 3: $\tilde{\omega} = 1.2$. The phase shift is clearly illustrated by the Lissajous curves (see Fig. 5).

- At low frequency ($\tilde{\omega} = 0.5$).
  The positive work region is slightly larger than the negative work region. As the excitation frequency goes smaller, the net input tends to be naught. The displacement response and the base vibration have a phase difference of ∼0°.
- At high frequency ($\tilde{\omega} = 1.2$).
  The net mechanical energy that inputs to the mechanical system tends to be naught, too. The displacement response and the base vibration have a phase difference of ∼180°.
- At resonance frequency ($\tilde{\omega} = 1$).
  The maximum input power happens while the base velocity and the response acceleration are in phase. That is the displacement response and the base vibration has a 90° phase difference. There is almost no negative work occurred in this situation.

The excitation does positive work to the energy harvesting system (W^+); it also does negative work to the energy harvesting system (W^-). That means actually not all mechanical energy input to the system is utilized (damping heat & converted electrical energy), but some of them flows back the excitation source. The net input mechanical energy is W^+–W^-.

The net power is from the constant term which is determined by the phase difference. At the resonance state (phase angle 90°), almost no energy flows back to the excitation source and all mechanical energy is used by the PEH. When the excitation frequency is far from the natural frequency of the PEH, the negative and positive work cancels each other and there is a very little amount of power input to the system, for compensating a variety of damping loss. For base-excited vibration systems, it is inevitable to do negative work for a certain period in each cycle in off-resonance conditions. Nevertheless ways to sustain a 90° phase gap between the excitation and response are worth exploring.

Work done by the external excitation on the system per cycle $T = \frac{2\pi}{2\omega}$ can be derived as

$$\begin{aligned} W &= \int_0^{\frac{2\pi}{2\omega}} P_{in}dt = \frac{\pi}{2}m\omega_n^2 A X_{ap}\sin(\phi_x) \\ &= \frac{\pi}{\omega}\frac{1}{2}m \times \left(\ddot{X}\right)_{amp} \times \left(\dot{Z}\right)_{amp}\sin(\phi_x), \end{aligned} \tag{28}$$

where $\phi_x \in [0° \ 180°]$. The work done by the external excitation is always positive.

The input mechanical energy is proportional to the mass, response acceleration, excitation velocity, and is directly related to the phase difference. The phase term $\sin(\phi_x)$ peaks at resonance and plunges once excitations deviate from resonance, as shown in Fig. 6. At the resonance state $\sin(\phi_x) = 1$, we can easily calculate the input energy by just measuring the excitation and response velocity/acceleration.

3.6. Efficiency

As aforementioned, efficiency is the ratio of the net output electrical energy (Eq. (25)) to the net input mechanical energy (Eq. (28)).

$$\eta = \frac{E_{out}}{W} = \frac{V_{RMS}^2 \Big/ R}{\frac{1}{2}m \times \left(\ddot{X}\right)_{amp} \times \left(\dot{Z}\right)_{amp}\sin(\phi_x)}. \tag{29}$$

Eq. (29) interprets the definition of efficiency, and it can be applied to different energy harvesters under base excitations.

For the defined linear system, we have

$$\eta = \frac{\kappa^2}{2\xi\tilde{\omega}\left(\frac{1}{r} + r\right) + \kappa^2} = \frac{\kappa^2}{2\frac{\xi}{\alpha}\tilde{\omega}^2 + 2\xi\alpha + \kappa^2}. \tag{30}$$

Efficiency is mainly related to the electromechanical coupling effect, damping effect, excitation frequency and electrical load. It

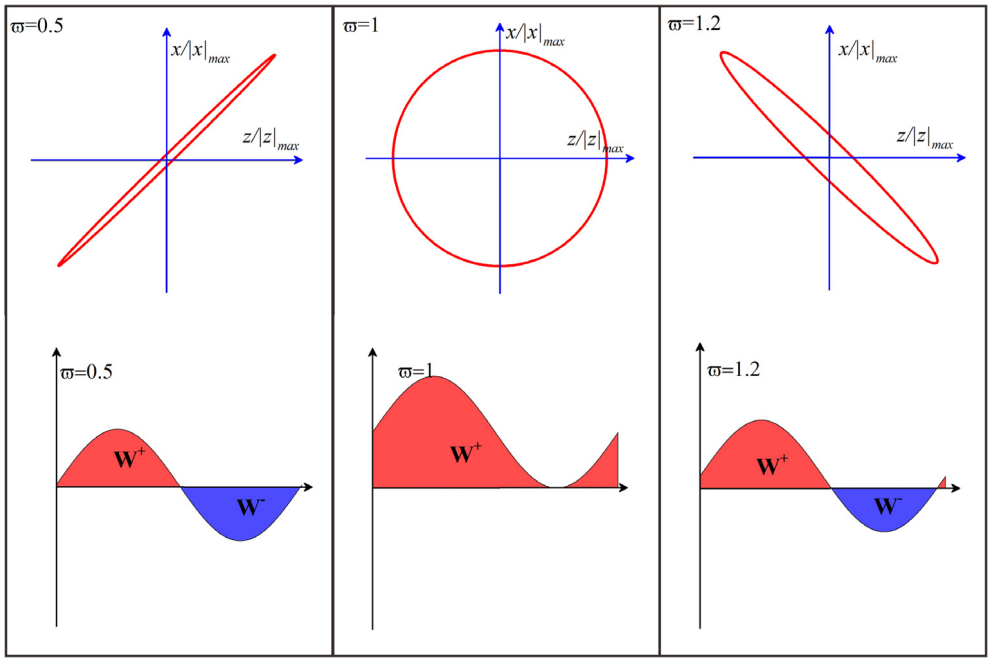

Fig. 5. Phase shift illustration and energy flow of a PEH system. The red region denotes that energy flows to the energy harvesting system, named "positive work" here; the blue region denotes that energy flow is from the energy harvesting system to the outside, named "native work" here. ($\phi_x = 0.0563;\ 1.57;\ 2.9189$). (For interpretation of the references to color in this figure legend, the reader is referred to the web version of this article.)

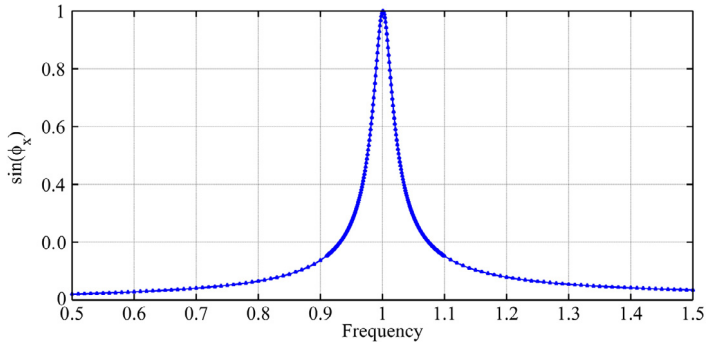

Fig. 6. Variations of $\sin(\phi_x)$ at different excitation frequency points.

is noteworthy that here κ^2 is also related to the structural stiffness and the capacitance of the employed piezoelectric element. Therefore, to gain a high efficiency, we need take full consideration of the structure, material, excitation and electrical load.

The maximum efficiency occurs while the resistance ratio $r = 1/RC_p\omega = 1$. However, to keep $r = 1$ at different frequency points, we have to actively adjust the load resistance, which requires great efforts and may consume energy. Usually in experiments, a fixed-value load resistance $R = 1/C_p\omega_n$ is selected. If more complex conditioning circuits are added, the expression of efficiency and optimum impedance will be changed. For example, if a full bridge rectifier and a smoothing capacitor are added between the PEH and the load resistor, the resistance ratio for the maximum efficiency and power output is $r = \frac{\pi}{2}/RC_p\omega$.

4. Experimental validation

To validate the defined efficiency, we have fabricated a prototype as shown in Fig. 7, which specifications are listed in Table 2. The active material used here is soft piezoceramic PZT-5A. The static capacitance C_p and loss $\tan\delta$ were measured to be 13.18 nF and 0.015, respectively. Fig. 7 shows the experimental platform. The PEH prototype was mounted vertically on an electromagnetic shaker that supplied a harmonic excitation while operating. Excitation parameters were set via a PC interface and loaded to a controller. The controller regulated the vibration of the shaker via a signal amplifier based on the instructions from the PC and the feedback signal from an accelerometer. The electrical and mechanical responses were monitored using an oscilloscope and a laser Doppler vibrometer, respectively. All experiments were conducted on a vibration isolation platform to reduce unwanted interference. The excitation acceleration was maintained constant at 0.3 g ($g = 9.8\ \mathrm{m/s^2}$) in the testing.

To calculate the efficiency of the PEH using Eq. (29), we first need to identify the involved parameters. The equivalent mass m of the structure can be roughly calculated with

$$m = \frac{33}{140}M_{beam} + M_{tip}. \tag{31}$$

The equivalent mass of the fabricated prototype is $m = 16.4$ g. The coupling coefficient is $= 0.0883$, decided using the experimental method. The damping ratio of the system is $\xi = 0.021$, which was determined using the logarithmic decrement method. [49]. By doing the frequency-sweep testing, we find that there is not a big difference between the open-circuit resonance frequency and the short-circuit one of the constructed system;

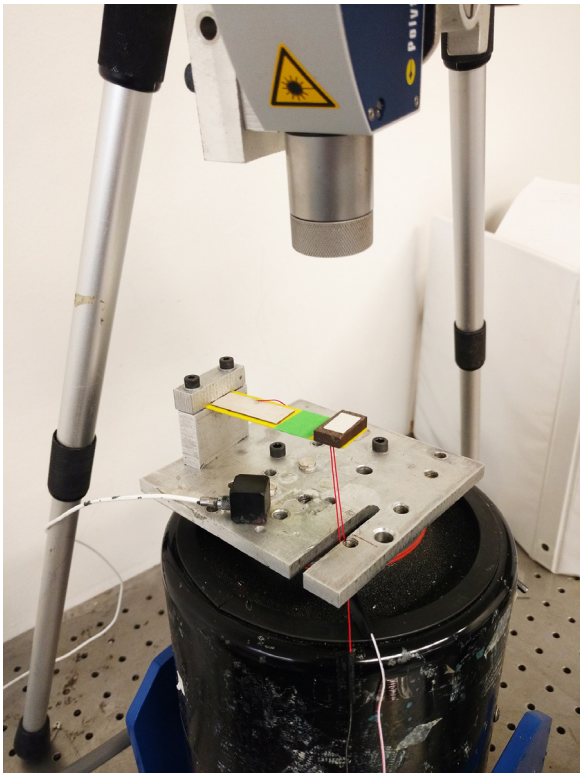

Fig. 7. Experimental setup and the fabricated prototype.

Table 2
Geometric and material properties of the PEH prototype.

Name	Value
Substructure length	73 mm
Substructure width	21 mm
Substructure thickness	0.5 mm
Substructure Young's modulus	69 GPa
Substructure density	2.73 g/cm^3
Piezo plate length	37.6 mm
Piezo plate width	15.1 mm
Piezo plate thickness	0.50 mm
Tip mass	15.6 g
Dielectric constant ϵ_{11}	1680
Piezoelectric charge constant, d_{31}	$-180 * 10^{-12}$ C/N
Piezoelectric voltage constant, g_{31}	$-11.3 * 10^{-3}$ Vm/N

both are around 28.4 Hz ($\omega_n = 178.6$). The matching resistance $R = 400$ kΩ is identified following the method in Ref. [49]. The resistance was kept constant in the whole experiments. With these parameters in hand, we can calculate the efficiency value of the system via Eq. (30).

We got the voltage data from the oscilloscope and used Eq. (25) to calculate the electrical energy per cycle. To get input mechanical energy, the relative acceleration and base velocity are needed. We used the laser vibrometer to measure the absolute velocity of the tip mass and base velocity, and derived the input mechanical energy at each frequency point. The tests have been repeatedly conducted for many times to ensure the validity and accuracy of the measured data.

Fig. 8 shows the measured efficiency compared with the estimated value. The comparison indicates that the developed theory can estimate efficiency very well. The efficiency of the fabricated PEH is about 6%–12%. Both experimental and theoretical studies manifest that the energy conversion efficiency of energy harvesters tends to decrease as the excitation frequency rises. Efficiency values of off-resonance states are not always much lower than those of the on-resonance states. For example, the efficiency is about 11% at 20 Hz in this case as shown in Fig. 8, which is higher than that (<10%) at the resonant state (28 Hz). Also, one should note that conditions to attain the maximum power transfer (around resonant points) do not coincide with conditions to achieve the highest energy conversion efficiency.

The phase difference between the excitation and the system response is observed in experiments, which matches the model estimation (Fig. 4). As shown in Fig. 9, in low-frequency conditions, the response tends to keep a same pace with the base excitation. When it comes to resonance, roughly a 90° phase lag appears. In high-frequency conditions, the response lags behind the excitation about 180°. That means when the host goes to one direction, the tip mass of the PEH, instead of following the excitation, moves to the opposite direction.

5. Linear systems

5.1. Validation via the energy flow analysis

From the perspective of energy flow, the mechanical energy in the energy harvesting system finally is consumed by the damping effects and extracted by the external load. Therefore we should have $W = E_{out} + W_{damping}$. This formula has been used to analyze efficiency of energy harvesters as aforementioned. Here, we examine if the derived efficiency expression meets this deduction.

$$E_{out} = \int_0^{\frac{2\pi}{2\omega}} P_{out}\,dt = \frac{\pi}{2}\frac{\theta^2}{C_p}\frac{r}{1+r^2}X_{ap}^2 \tag{32}$$

$$W_{damping} = \int_0^{\frac{2\pi}{2\omega}} c\dot{X}^2 dt = \frac{\pi\omega}{2}cX_{ap}^2 \tag{33}$$

$$\begin{aligned} W &= \frac{\pi}{2}m\omega_n^2 A X_{ap}\sin(\phi_x) \\ &= \frac{\pi}{2}m\omega_n^2 A X_{ap}\frac{1}{\sqrt{\Lambda}}\tilde{\omega}\left(2\xi + \frac{\alpha\kappa^2}{\tilde{\omega}^2+\alpha^2}\right) \\ &= \frac{\pi}{2}m\omega_n^2\tilde{\omega}\left(2\xi + \frac{\alpha\kappa^2}{\tilde{\omega}^2+\alpha^2}\right)X_{ap}^2 \\ &= \left(\frac{\pi}{2}m\tilde{\omega}2\xi + \frac{\pi}{2}m\frac{r\kappa^2}{1+r^2}\right)\omega_n^2 X_{ap}^2 \\ &= \left(\frac{\pi}{2}\omega c + \frac{\pi}{2}\frac{\theta^2}{C_p}\frac{r}{1+r^2}\right)X_{ap}^2 \\ &= W_{damping} + E_{out}. \end{aligned} \tag{34}$$

The derived efficiency expression is validated from the perspective of the energy flow.

5.2. Parametric study

According to Eq. (30), efficiency is mainly affected by the load resistance, damping and electromechanical coupling effect. Next, we talk about the effects of these parameters on efficiency.

As illustrated in Fig. 10, load resistance has a significant effect on the energy conversion efficiency. As the load resistance increases, the efficiency peaks around the matching resistance points (resistance ratio $r = 1$), and then drops dramatically. With a same resistance, a PEH under a low-frequency excitation shows high efficiency.

Fig. 11 Shows the effect of the structural damping on efficiency in both on- and off-resonance states.

Efficiency variation becomes increasingly small as damping ascends. That means the efficiency value tends to keep constant, uncorrelated to damping variation once damping turns strong.

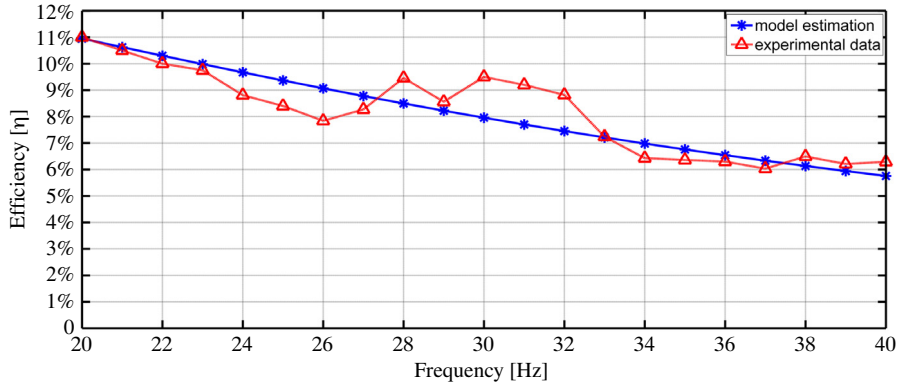

Fig. 8. Efficiency at different frequency points collocated from the experimental data and estimated by the developed model. The resonance frequency is about 28 Hz.

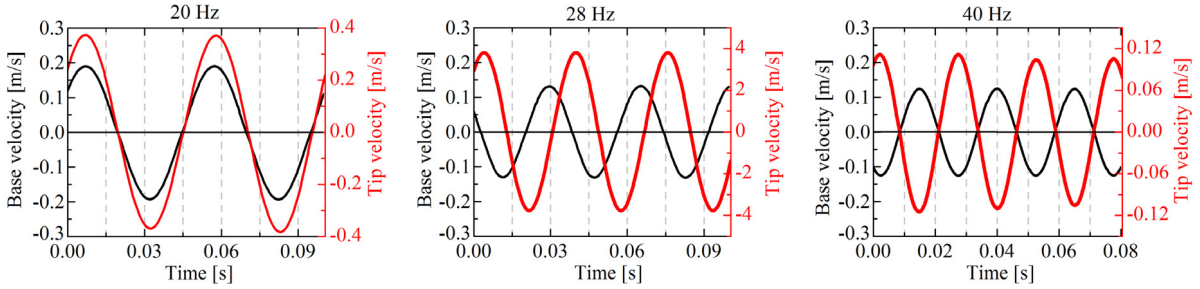

Fig. 9. Velocity responses of the tip end and the base of the PEH under different excitations. Black line: base velocity; red line: tip velocity. (For interpretation of the references to color in this figure legend, the reader is referred to the web version of this article.)

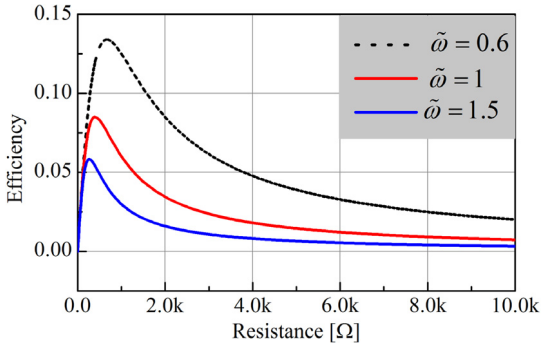

Fig. 10. Effect of the load resistance on efficiency. ($\kappa^2 = 0.0078$, $\zeta = 0.021$).

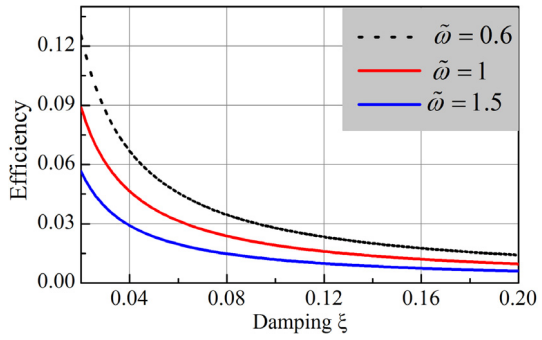

Fig. 11. Damping effect on efficiency ($\kappa^2 = 0.0078$, $\alpha = 1$).

Also, the coupling coefficient κ^2 plays a decisive role in the exhibited efficiency of a PEH. Fig. 12 illustrates the effect of the coupling coefficient on efficiency. As expected, the higher the coupling coefficient is, the more efficiently the PEH behaves. The slopes of the response curves get increasingly larger as we increase k^2. That means for systems with a weak coupling effect, efficiency

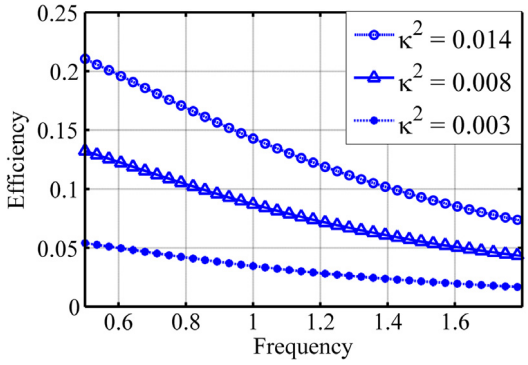

Fig. 12. Effect of the coupling coefficient on efficiency ($\alpha = 1$, $\zeta = 0.021$).

is prone to keep unchanged as the excitation frequency varies. In contrast, systems with a relatively strong coupling effect, the efficiency value experiences a big difference. It is worth noting that the coupling coefficient is inversely proportional to the structural stiffness and the internal piezoelectric capacitance. Thus, designs with soft structures and small internal capacitance tend to exhibit high efficiency.

6. Nonlinear systems

As discussed before, linear systems experience a 90° phase difference at resonance states and shift phase nearly 180° when frequency is much higher than the resonant one. We can utilize this characteristic to obtain the efficiency value of linear energy harvesters. To broaden the frequency bandwidth, researchers have introduced nonlinear vibration into energy harvesting systems [15,43,64,65] It is unclear whether the phase difference of these nonlinear systems will match the linear ones.

To study the phase shift phenomenon in nonlinear PEHs, we constructed two prototypes as shown in Fig. 13. The nonlinear

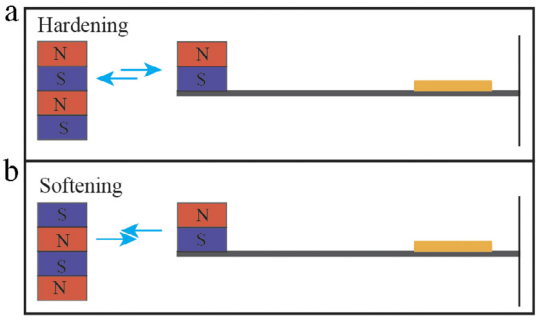

Fig. 13. Nonlinear PEHs: (a) hardening, (b) softening.

magnetic force was utilized to provoke nonlinear dynamic responses. By adjusting the magnet layout, we achieved both hardening and softening nonlinear responses. When there is a soft repulsive force between the moving and fixed magnets, the system shows the hardening nonlinearity; when there is an attractive force between the moving and the fixed magnets, the system shows the softening nonlinearity.

The prototype was fabricated with a high carbon spring steel beam of 70 × 7 × 0.25 mm^3. As shown in Fig. 13, a small piezoelectric element was attached near to the fixed end of the steel beam (13.7 mm to the end). The piezoelectric element was made of PZT-5A and its dimension is 7 × 8 × 0.2 mm^3. A Neodymium magnet (ϕ8.31 × 2 mm) (Grade N42) was attached at the free end of the steel beam, facing a pair of same-size magnets fixed on the base. The experiments were conducted on the platform described before, and the excitation frequency was swept upward and downward with a constant rate of 0.1 Hz/s.

Take the upward frequency-sweep case of the hardening nonlinear PEH for example, as the excitation frequency rises constantly from 10 Hz, we can see a slight increase in the velocity response. When the excitation frequency approaches to the resonance (20.4 Hz), the response starts to increases quickly. Once it passes the resonant frequency (i.e., jump frequency), the response jumps down and decreases slowly ever since. The phase difference, likewise, keeps nearly zero at frequency points before the resonance and quickly passes 90° and rises to ∼180° while the frequency is swept through the resonance. For the downward frequency-sweep case, the phase difference stays around 180° and drops quickly to 0° around the jump-up frequency point (∼18.5 Hz). It is noticeable that a distinct hysteresis loop exists in the nonlinear systems, which is not observed in the linear systems. The softening nonlinear system shows a same type of phase shift as the hardening nonlinear system. Comparing the phase angle figures of linear systems (Fig. 4) and nonlinear systems (Fig. 14), we find that linear and nonlinear systems act in a very similar way and all reverse around the resonance points. The former energy flow analysis can also be applied to the nonlinear systems.

For both hardening and softening nonlinear PEHs, there exists a roughly 90° phase shift between excitations and responses around the jump points. Consequently, we can easily calculate the input mechanical energy and further efficiency using Eq. (29).

7. Discussions

We have presented a comprehensive framework for discussing the efficiency of piezoelectric energy harvesters. Parameters that affect the harvesters' efficiency have been identified and quantitatively analyzed. It is noted that efficiency is directly related to the phase difference between excitation and response, which complicates the efficiency calculation.

In order to take advantage of the unique 90° phase shift at resonance, we suggest comparing different PEHs at the resonance states while evaluating their efficiency values. The reasons are as follows.

1. The on-resonance efficiency is easy to be calculated experimentally and theoretically.
2. To generate high-power output, most PEHs are designed to work around the resonance states. Therefore, the on-resonance efficiency reflects the real working performance well.
3. Efficiency has an approximate monotonically decreasing relationship with the excitation frequency. Consequently, efficiency values at other points can be extrapolated with the on-resonance efficiency in hand.

Note that the resonance state here means the point of the maximum power output. It is known that optimal power output conditions (frequency, resistance, damping, etc.) do not coincide with those of the optimal efficiency, especially for strongly-coupling systems. As the analysis and experiments indicate, systems with weak damping effects and low-frequency excitations always show high efficiency, regardless the energy harvesting capability. Therefore, it is more reasonable to discuss efficiency values at the maximum power output conditions, not at the optimal efficiency points.

It is worth noting that solely pursuing maximum efficiency may result in a significant drop on power output, and misguide the development of new PEHs. When evaluating different PEHs, we suggest to use a set of figures of merit, including efficiency, power density, excitation-normalized power density, frequency bandwidth, etc., instead of one performance metric. Meanwhile, the working conditions such as volume, mass and excitation strength ought to be considered seriously.

8. Summary

In this paper, we theoretically and experimentally studied PEHs' efficiency of converting mechanical input energy to electrical energy dissipated by a load resistance. We reviewed representative work on efficiency and analyzed the energy flow in the energy harvesting process. We derived an analytical efficiency expression based on a SDOF model for the most commonly used cantilever PEHs, and validated the efficiency expression experimentally. The study indicates that efficiency is mainly related to the electromechanical coupling effect, damping effect, excitation frequency and electrical load. Light damping and strong coupling effects help improve efficiency. In contrast, both small and large resistors lead to a significant drop in efficiency; efficiency peaks with a modest matching impedance. Both experimental and theoretical studies show that the energy conversion efficiency decreases as the excitation frequency increases.

Depending on the period of time in each cycle, the work done by the excitations on the PEHs can either be positive or negative, which is characterized by the phase difference between excitations and responses. The phase shifts nearly 180° as the excitation frequency ramps up and down. Around the resonance frequency, a phase difference is 90° for both linear PEHs and nonlinear PEHs. A 90° phase difference means the excitation always does positive work in each working period. This characteristic yields exceptional convenience in calculating the efficiency value of the energy conversion process. Efficiency at resonance states reflects the real working performance well and is easily calculated. Therefore, while discussing different PEHs we suggest to use the efficiency at the resonance condition.

Acknowledgment

This work was supported by the Natural Science and Engineering Research Council of Canada.

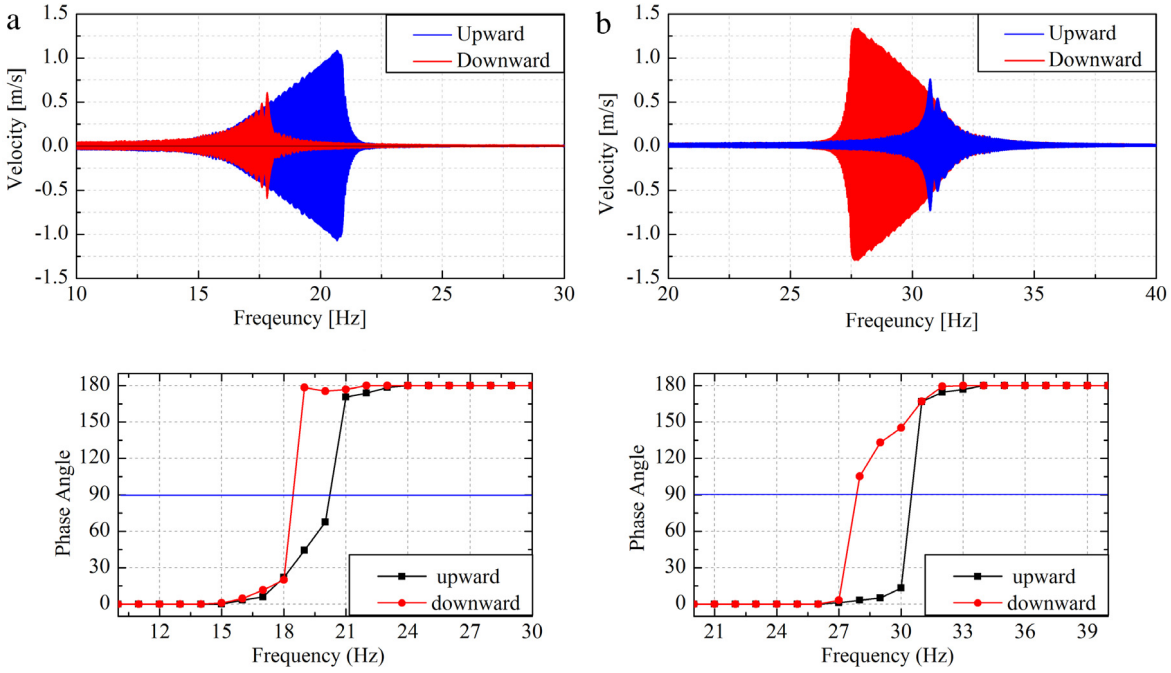

Fig. 14. Experimental amplitude and phase responses of the hardening and softening nonlinear PEHs. Both experiments were done with a constant excitation of 0.2 g acceleration. (a) The hardening system is under an excitation of 10–30 Hz; (b) the softening system is under an excitation of 20–40 Hz.

References

[1] C. Bowen, M. Arafa, Energy harvesting technologies for tire pressure monitoring systems, Adv. Energy Mater. 5 (7) (2015).
[2] O. Brand, et al., Micro Energy Harvesting, John Wiley & Sons, 2015.
[3] C. Dagdeviren, et al., Conformal piezoelectric energy harvesting and storage from motions of the heart, lung, and diaphragm, Proc. Natl. Acad. Sci. 111 (5) (2014) 1927–1932.
[4] Z. Yang, J. Zu, Comparison of PZN-PT, PMN-PT single crystals and PZT ceramic for vibration energy harvesting, Energy Convers. Manage. 122 (2016) 321–329.
[5] M.H. Malakooti, et al., ZnO nanowire interfaces for high strength multifunctional composites with embedded energy harvesting, Energy Environ. Sci. 9 (2) (2016) 634–643.
[6] G.T. Hwang, et al., Self - powered cardiac pacemaker enabled by flexible single crystalline PMN - PT piezoelectric energy harvester, Adv. Mater. 26 (28) (2014) 4880–4887.
[7] G.T. Hwang, et al., A reconfigurable rectified flexible energy harvester via solid - state single crystal grown PMN–PZT, Adv. Energy Mater. 5 (10) (2015).
[8] R.A. Whiter, V. Narayan, S. Kar - Narayan, A scalable nanogenerator based on self - poled piezoelectric polymer nanowires with high energy conversion efficiency, Adv. Energy Mater. 4 (18) (2014).
[9] Z. Yang, J. Zu, High-efficiency compressive-mode energy harvester enhanced by a multi-stage force amplification mechanism, Energy Convers. Manage. 88 (2014) 829–833.
[10] T.-B. Xu, et al., Energy harvesting using a PZT ceramic multilayer stack, Smart Mater. Struct. 22 (6) (2013) 065015.
[11] X. Wang, et al., A frequency and bandwidth tunable piezoelectric vibration energy harvester using multiple nonlinear techniques, Appl. Energy 190 (2017) 368–375.
[12] W. Zhou, G.R. Penamalli, L. Zuo, An efficient vibration energy harvester with a multi-mode dynamic magnifier, Smart Mater. Struct. 21 (1) (2012) 015014.
[13] G.T. Hwang, et al., Self - powered wireless sensor node enabled by an aerosol - deposited PZT flexible energy harvester, Adv. Energy Mater. 6 (13) (2016).
[14] A. Koka, H.A. Sodano, A low - frequency energy harvester from ultralong, vertically aligned BaTiO3 nanowire arrays, Adv. Energy Mater. 4 (11) (2014).
[15] Z. Yang, J. Zu, Z. Xu, Reversible Nonlinear Energy Harvester Tuned by Tilting and Enhanced by Nonlinear Circuits.
[16] A. Erturk, D. Inman, Broadband piezoelectric power generation on high-energy orbits of the bistable Duffing oscillator with electromechanical coupling, J. Sound Vib. 330 (10) (2011) 2339–2353.
[17] S. Zhou, et al., Broadband tristable energy harvester: modeling and experiment verification, Appl. Energy 133 (2014) 33–39.
[18] S.P. Beeby, et al., A micro electromagnetic generator for vibration energy harvesting, J. Micromech. Microeng. 17 (7) (2007) 1257.
[19] S. Roundy, On the effectiveness of vibration-based energy harvesting, J. Intell. Mater. Syst. Struct. 16 (10) (2005) 809–823.
[20] P.D. Mitcheson, et al., Architectures for vibration-driven micropower generators, J. Microelectromech. Syst. 13 (3) (2004) 429–440.
[21] P.D. Mitcheson, et al., Energy harvesting from human and machine motion for wireless electronic devices, Proc. IEEE 96 (9) (2008) 1457–1486.
[22] W.Q. Liu, et al., A new figure of merit for wideband vibration energy harvesters, Smart Mater. Struct. 24 (12) (2015) 125012.
[23] M. Kim, J. Dugundji, B.L. Wardle, Efficiency of piezoelectric mechanical vibration energy harvesting, Smart Mater. Struct. 24 (5) (2015) 055006.
[24] J. Xie, et al., A piezoelectric energy harvester based on flow-induced flexural vibration of a circular cylinder, J. Intell. Mater. Syst. Struct. 23 (2) (2012) 135–139.
[25] M.W. Shafer, E. Garcia, The power and efficiency limits of piezoelectric energy harvesting, J. Vib. Acoust. 136 (2) (2014) 021007.
[26] Q. Wang, N. Wu, Optimal design of a piezoelectric coupled beam for power harvesting, Smart Mater. Struct. 21 (8) (2012) 085013.
[27] Y. Shu, I. Lien, Efficiency of energy conversion for a piezoelectric power harvesting system, J. Micromech. Microeng. 16 (11) (2006) 2429.
[28] L. Xiangjian, C. Renwen, Z. Liya, Energy conversion efficiency of rainbow shape piezoelectric transducer, Chin. J. Aeronaut. 25 (5) (2012) 691–697.
[29] C. Chang, et al., Direct-write piezoelectric polymeric nanogenerator with high energy conversion efficiency, Nano Lett. 10 (2) (2010) 726–731.
[30] H.W. Kim, et al., Energy harvesting using a piezoelectric "cymbal" transducer in dynamic environment, Japan. J. Appl. Phys. 43 (2004) 6178.
[31] S. Jiang, Y. Hu, Analysis of a piezoelectric bimorph plate with a central-attached mass as an energy harvester, IEEE Trans. Ultrason. Ferroelectr. Freq. Control 54 (7) (2007) 1463–1469.
[32] H.A. Sodano, D.J. Inman, G. Park, Comparison of piezoelectric energy harvesting devices for recharging batteries, J. Intell. Mater. Syst. Struct. 16 (10) (2005) 799–807.
[33] H.D. Akaydin, N. Elvin, Y. Andreopoulos, The performance of a self-excited fluidic energy harvester, Smart Mater. Struct. 21 (2) (2012) 025007.
[34] M.W. Shafer, M. Bryant, E. Garcia, Designing maximum power output into piezoelectric energy harvesters, Smart Mater. Struct. 21 (8) (2012) 085008.
[35] A. Bayrashev, Robbins W P, B. Ziaie, Low frequency wireless powering of microsystems using piezoelectric–magnetostrictive laminate composites, Sensors Actuators A 114 (2) (2004) 244–249.
[36] P. Janphuang, et al., On the experimental determination of the efficiency of piezoelectric impact-type energy harvesters using a rotational flywheel, in: Journal of Physics: Conference Series, IOP Publishing, 2013.
[37] S.K. Karan, et al., An approach to design highly durable piezoelectric nanogenerator based on self - poled PVDF/AlO - rGO flexible nanocomposite with high power density and energy conversion efficiency, Adv. Energy Mater. (2016).
[38] J. Cho, et al., Efficiency of energy conversion by piezoelectrics, Appl. Phys. Lett. 89 (10) (2006) 4107.
[39] M. Umeda, K. Nakamura, S. Ueha, Analysis of the transformation of mechanical impact energy to electric energy using piezoelectric vibrator, Japan. J. Appl. Phys. 35 (5S) (1996) 3267.
[40] S. Crossley, S. Kar-Narayan, Energy harvesting performance of piezoelectric ceramic and polymer nanowires, Nanotechnology 26 (34) (2015) 344001.
[41] G.A. Lesieutre, C.L. Davis, Can a coupling coefficient of a piezoelectric device be higher than those of its active material? in: Smart Structures and Materials'97, International Society for Optics and Photonics, 1997.
[42] C.D. Richards, et al., Efficiency of energy conversion for devices containing a piezoelectric component, J. Micromech. Microeng. 14 (5) (2004) 717.

[43] R.L. Harne, K.W. Wang, A review of the recent research on vibration energy harvesting via bistable systems, Smart Mater. Struct. 22 (2) (2013) 023001.
[44] M. Goldfarb, L.D. Jones, On the efficiency of electric power generation with piezoelectric ceramic, J. Dyn. Syst. Meas. Control 121 (3) (1999) 566–571.
[45] M. Renaud, et al., Optimum power and efficiency of piezoelectric vibration energy harvesters with sinusoidal and random vibrations, J. Micromech. Microeng. 22 (10) (2012) 105030.
[46] Y. Liao, H.A. Sodano, Structural effects and energy conversion efficiency of power harvesting, J. Intell. Mater. Syst. Struct. (2009).
[47] H.A. Sodano, G. Park, D. Inman, Estimation of electric charge output for piezoelectric energy harvesting, Strain 40 (2) (2004) 49–58.
[48] N.E. Dutoit, B.L. Wardle, S.-G. Kim, Design considerations for MEMS-scale piezoelectric mechanical vibration energy harvesters, Integr. Ferroelectr. 71 (1) (2005) 121–160.
[49] Z. Yang, Y. Zhu, J. Zu, Theoretical and experimental investigation of a nonlinear compressive-mode energy harvester with high power output under weak excitations, Smart Mater. Struct. 24 (2) (2015) 025028.
[50] J. Liang, W.-H. Liao, Energy flow in piezoelectric energy harvesting systems, Smart Mater. Struct. 20 (1) (2010) 015005.
[51] N.W. Hagood, W.H. Chung, A. Von Flotow, Modelling of piezoelectric actuator dynamics for active structural control, J. Intell. Mater. Syst. Struct. 1 (3) (1990) 327–354.
[52] Y. Shu, I. Lien, Analysis of power output for piezoelectric energy harvesting systems, Smart Mater. Struct. 15 (6) (2006) 1499.
[53] N.E. DuToit, B.L. Wardle, Experimental verification of models for micro-fabricated piezoelectric vibration energy harvesters, AIAA J. 45 (5) (2007) 1126–1137.
[54] G.K. Ottman, et al., Adaptive piezoelectric energy harvesting circuit for wireless remote power supply, IEEE Trans. Power Electron. 17 (5) (2002) 669–676.
[55] G.D. Szarka, B.H. Stark, S.G. Burrow, Review of power conditioning for kinetic energy harvesting systems, IEEE Trans. Power Electron. 27 (2) (2012) 803–815.
[56] D. Guyomar, et al., Toward energy harvesting using active materials and conversion improvement by nonlinear processing, IEEE Trans. Ultrason. Ferroelectr. Freq. Control 52 (4) (2005) 584–595.
[57] L. Garbuio, et al., Mechanical energy harvester with ultralow threshold rectification based on SSHI nonlinear technique, IEEE Trans. Ind. Electron. 56 (4) (2009) 1048–1056.
[58] E. Lefeuvre, et al., Piezoelectric energy harvesting device optimization by synchronous electric charge extraction, J. Intell. Mater. Syst. Struct. 16 (10) (2005) 865–876.
[59] Y. Wu, et al., Piezoelectric vibration energy harvesting by optimized synchronous electric charge extraction, J. Intell. Mater. Syst. Struct. 24 (12) (2013) 1445–1458.
[60] Y.K. Ramadass, A.P. Chandrakasan, An efficient piezoelectric energy harvesting interface circuit using a bias-flip rectifier and shared inductor, IEEE J. Solid-State Circuits 45 (1) (2010) 189–204.
[61] J. Dicken, et al. Single-supply pre-biasing circuit for low-amplitude energy harvesting applications, in: Proceedings of PowerMEMS, 2011, pp. 46–49.
[62] T. Hehn, Y. Manoli, CMOS Circuits for Piezoelectric Energy Harvesters, in: Springer Series in Advanced Microelectronics, vol. 38, 2015, pp. 21–40.
[63] S.S. Rao, Mechanical Vibrations 5th edition SI, Pearson, Singapore, 2011.
[64] R. Masana, M.F. Daqaq, Electromechanical modeling and nonlinear analysis of axially loaded energy harvesters, J. Vib. Acoust. 133 (1) (2011) 011007.
[65] S.C. Stanton, C.C. McGehee, B.P. Mann, Nonlinear dynamics for broadband energy harvesting: Investigation of a bistable piezoelectric inertial generator, Physica D 239 (10) (2010) 640–653.